PAPER

Check for updates

Fabrication of core–shell type poly(NIPAm)-encapsulated citral and its application on bamboo as an anti-molding coating†

Rui Peng, [ID] Chungui Du, [ID] * Ailian Hu, Qi Li, Jingjing Zhang, Weigang Zhang and Fangli Sun

Bamboo is a widely used renewable and degradable biomass material; however, its sustainable utilisation is hindered by its susceptibility to mold. The current bamboo anti-mold technology is mainly based on organic chemical agents; these agents can easily induce mold resistance in bamboo with long-term use, and can even adversely affect human health. In the present study, the poly(*N*-isopropyl acrylamide) (PNIPAm)/ citral nanohydrogel was prepared by encapsulating the natural antibiotic citral in PNIPAm for the anti-mold treatment of bamboo. The results revealed that this nanohydrogel exhibited a core–shell system with citral as the 'core' and PNIPAm as the 'shell', an average hydrodynamic diameter of 88.1 nm, and a low critical solution temperature (LCST) of 35.4 °C. After the high-pressure impregnation with the nanohydrogel, the bamboo strips showed excellent control effects toward common bamboo molds. Therefore, the nanohydrogel demonstrated high efficiency and it may become an ideal alternative to organic chemical anti-mold agents, thus showcasing its significant potential in the field of mold prevention for bamboo.

1. Introduction

Biomass materials are the only renewable and sustainable materials among the four modern basic materials (*i.e.* steel, cement, plastic, and biomass materials).[1–3] Bamboo, one of the biomass materials, has demonstrated significant advantages in terms of structure, cost, and environmental sustainability. Moreover, its tensile strength is comparable to that of low carbon steel, and it exhibits excellent toughness and degradability,[4–6] which make it widely popular for use in construction, food, decoration, furniture, garden, and other fields.[7–11] However, the nature of bamboo makes it prone to mold and decay, which suppresses the advantages of hardness and strength, resulting in the decrease or loss of its application value.[12,13] As the country with the largest bamboo production in the world, China's annual bamboo loss due to mold and decay is as high as 10% of the gross output.[14] Considering the bamboo production of 3.155 billion in 2018, more than 300 million bamboos have been lost, which has resulted in an economic loss of >3 billion renminbi (RMB).[15,16] Despite the decay resistance property of bamboo, the problem of durable mold resistance in bamboo remains unsolved to date, which has become the bottleneck for the sustainable development of the bamboo

industry. Therefore, in-depth and systematic research on the long-term resistance of bamboo to mold is urgently required. Some scholars have studied the anti-mold agents of bamboo and have achieved a wealth of results.[17–19] Chemical agents remain the dominant bamboo anti-mold agents; however, they easily cause drug resistance in mold, as well as show poor environmental performance, which may cause harm to human health and the environment in the long term.[20–22] Therefore, it is necessary to develop a novel bamboo anti-mold agent that does not easily produce drug resistance or challenge environmental safety, and is consistent with the inevitable requirements and development direction in bamboo mold-proof research.

Recently, a citral source from the essential oil of *Litsea cubeba* has attracted great attention owing to the low drug resistance, strong antimicrobial activity, broad antibacterial spectrum, and environmental-friendliness of citral.[23–25] The United States Food and Drug Administration has approved its use in food. This product can damage the cell morphology of fungi such as *Aspergillus flavus* and *Penicillium dactyloides* by damaging their mitochondria, and hence, it has become the focus of antifungal research in the food, cosmetics, and medical industries.[22,26,27] Therefore, it is believed that a citral bamboo anti-mold agent would be eco-friendly, safe, and show superior anti-mold effect. However, owing to the limitations of high hydrophobicity and easy degradation and volatilisation of citral, its application in the field of anti-mold agents of bamboo is hampered by significant challenges.[28–30] Notably, the results of studies by Natrajan[29] and Tian[31] have confirmed that the

College of Chemistry and Materials Engineering, Zhejiang A & F University, Hangzhou 311300, Zhejiang, China. E-mail: chunguidu@163.com

encapsulation of citral with nanocarriers can be extremely effective in improving the solubility, stability, and biological distribution of citral.

Among the numerous nanocarriers known, poly (*N*-isopropyl acrylamide) (PNIPAm) nanohydrogel has demonstrated remarkable outcomes. This smart hydrogel having an integrating three-dimensional network structure, nanometre properties, and thermal responsiveness can be dispersed stably in water. Moreover, due to the presence of a large number of active sites that can combine with other functional components, they are often used as intelligent carriers for drug delivery systems.[32–34] Consequently, the use of PNIPAm as a carrier to encapsulate citral is expected to effectively eliminate its drawbacks and facilitate the control of the release of citral to ultimately improve its stability, utilisation efficiency, and antibacterial activity, which in turn is believed to achieve the durable anti-mold effect of bamboo. The most critical technology for achieving this goal is encapsulation. Presently, the encapsulation methods for citral mainly include spray drying,[22,35] oil-in-water emulsions,[36,37] multilayer emulsion,[38] and molecular compounds.[28] However, these methods are associated with some limitations; the preparation cost involved in spray drying is high, the water-in-oil emulsion is easily affected by environmental stress factors, the preparation process of multilayer emulsion is extremely complex, and the development of molecular complexes requires a long time to balance. To this end, we propose a simple strategy of encapsulating citral in PNIPAm through soap-free emulsion polymerisation (SFEP), to obtain a nanohydrogel drug delivery system with citral, having thermal responsiveness and hydrophilicity. This nanoparticle hydrogel has a narrow particle size distribution, which eliminates the problems caused by organic solvents and surfactants that otherwise cause pollution and make removal difficult.[39] Furthermore, mild reaction conditions make the citral drug delivery system stable, which is conducive to industrial production.[40,41]

In our previous study, we found that the non-encapsulated citral exerts an excellent anti-mold effect when it directly acts on bamboo mold.[42] However, the drying treatment is involved after impregnating bamboo with citral. To ensure the protection of bamboo from mold, the concentration of citral must be significantly increased, considering the thermal instability of citral. Thus, the encapsulation of citral in PNIPAm has extremely important research significance and application prospects. To date, no report is available on the encapsulation of citral by PNIPAm and its application as a bamboo anti-mold agent. In the present study, the PNIPAm/citral nanohydrogel was prepared through SFEP, and the chemical composition, particle size, microstructure, and temperature sensitivity of the resultant product were characterised. Additionally, the anti-mold status and the mechanism of bamboo treatment with PNIPAm/citral were investigated. A schematic diagram of the experiments performed in the study is shown in Fig. 1. The effective barrier and thermal sensitivity of PNIPAm were used to control the release of citral, through which the effect of high efficiency and long-lasting resistance of the bamboo to mold could be achieved. This study provides a novel approach for the

realisation of long-term and efficient anti-mold effects of bamboo. Moreover, it lays the foundation and provides theoretical references for the popularisation and application of citral in the field of anti-mold agents of bamboo.

2. Materials and methods

2.1 Materials

N-Isopropylacrylamide (NIPAm, AR) was purchased from TCI Chemicals Co. Ltd., China. *N,N'*-Methylenebisacrylamide (MBA, AR), tetramethylenediamine (TMEDA, AR), potassium persulfate (KPS, AR), and polyethylene glycol monostearate (PEGMS, n = 45, AR) were supplied by Aladdin Reagent Co. China. Citral (*cis*-reverse isomer mixture, 97%), disodium hydrogen phosphate (AR), and sodium dihydrogen phosphate (AR) were all obtained from Sinopharm Chemical Reagents Co. Ltd. Anhydrous ethanol (AR) was provided by Tianjin Yongda Chemical Reagent Co. Ltd. Bamboo strips (moisture content of about 10%) were provided by Zhejiang Yongyu Bamboo Industry Co. Ltd., and made into uniform 50 mm × 20 mm × 5 mm strips in the laboratory. All the reagents and solvents were used directly without any further purification. Deionised water was prepared in the laboratory.

2.2 Preparation of the PNIPAm/citral nanohydrogel

PNIPAm nanohydrogel was first prepared through free radical polymerisation, according to a method described previously, and then appropriately adjusted.[39] Briefly, a 250 mL three-neck round-bottom flask containing 100 mL of deionised water was purged with high-purity N_2 at room temperature. Then, 0.750 g of NIPAm monomer, 0.038 g of MBA cross-linking agent, 0.038 g of KPS initiator, and 0.038 g of TMEDA catalyst were added. The polymerisation reaction was performed in N_2 atmosphere for 6 h, and, after the reaction, a clear and transparent PNIPAm nanohydrogel solution was obtained following overnight standing incubation. Second, 0.050 g of PEGMS was added to the PNIPAm solution (0.2 mmol L^{-1}, below the critical micelle concentration); once it was dissolved, citral was added for the encapsulation reaction. Finally, the solution was immersed in dialysis bags (MWCO: 8000–14 000) to remove the unreacted substances and obtain the PNIPAm/citral nanohydrogel solution, which was stored at room temperature for subsequent use.

2.3 The working curve

The maximum absorption wavelength (λ_{max}) of citral in anhydrous ethanol was determined using a UV-vis spectrophotometer (UV-1800).[43] Then, a standard solution of citral ethanol with a concentration of 2–8 μg mL^{-1} was prepared, and its absorbance value was determined at λ_{max} (the average value was measured after 3 parallel measurements of each sample) to obtain the standard curve of citral.[44]

2.4 Determination of citral

The citral content in the PNIPAm/citral nanohydrogel after dialysis was directly estimated to obtain the citral content encapsulated in the PNIPAm nanohydrogel. Briefly, 20 mL of
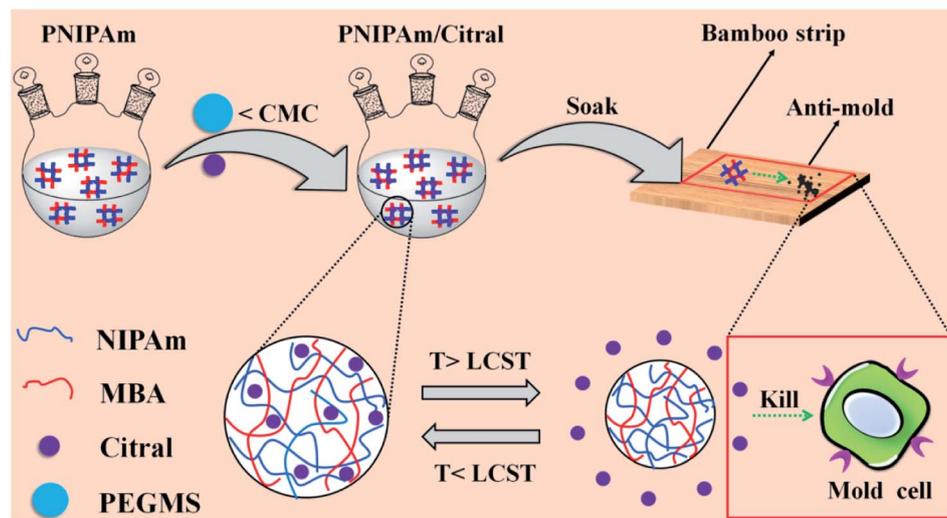
Fig. 1 The schematic diagram of the experimental study of the PNIPAm/citral nanohydrogel.

anhydrous ethanol was accurately measured in a 50 mL centrifuge tube, to which 0.5 mL of PNIPAm/citral nanohydrogel solution was added, and the mixture was centrifuged at 20 °C for 10 min at 15 000 rotation per min. Immediately after centrifugation, the supernatant was collected to determine the absorbance of citral (λ_{max}) using the UV-vis spectrophotometer. Finally, the mass of encapsulated citral was calculated from the standard curve of citral. The encapsulation efficiency of citral (EC) was calculated using the following formula (1):[45]

$$EC = \frac{L_2}{L_1} \times 100\% \tag{1}$$

where EC denotes the encapsulation efficiency of citral (%); L_1 denotes the initial addition amount of citral (mg), and L_2 denotes the mass of the encapsulated citral (mg).

2.5   Single-factor experiment

Considering the dosage of citral, reaction time, and reaction temperature as factors, the effects of each factor on the EC were investigated using a single-factor experiment. The dosages of citral were 10 mg, 20 mg, 30 mg, 40 mg, and 50 mg; the reaction times were 1 h, 2 h, 3 h, 4 h, and 5 h; and the reaction temperatures were 15 °C, 20 °C, 25 °C, 30 °C, and 35 °C.

2.6   Orthogonal experiment

Based on the results of the single-factor experiment, 3 levels corresponding to high, medium, and low results were selected for each factor. Orthogonal tests were designed in accordance with the $L_9(3^4)$ orthogonal test table. Finally, the experimental results were analysed.

2.7   Fourier-transform infrared spectroscopy

Freeze-dried PNIPAm/citral nanohydrogel samples were ground into powder, mixed with potassium bromide at a mass ratio of 1 : 100, and then pressed into thin slices. The molecular structure of the composite hydrogel was analysed through

Fourier-transform infrared spectroscopy (FT-IR) (IR Prestige-21). The resolution of FT-IR was 4 cm^{-1}, and the wavelength range was 4000–400 cm^{-1}. Each sample was scanned thrice, and the spectra needed to overlap at least twice.

2.8   Dynamic light scattering

Several drops of PNIPAM/citral nanohydrogel solution were placed in a quartz sample cell and diluted with deionised water. The bubbles in the solution were then removed through vibration. The particle size of the nanohydrogel was analysed through dynamic light scattering (DLS) (Zeta PALS-31484). The measurement conditions were as follows: transmitting laser, 658 nm; laser energy, 4.0 mW; background scattering, 173°; and temperature, 25 °C. Each sample was scanned 5 times, and the final results were averaged.

2.9   Transmission electron microscopy

After subjecting the PNIPAm/citral nanohydrogel solution to ultrasound for 10 min, it was dropped onto a 200-mesh copper mesh covered with a formvar film. After drying the film at room temperature, uranyl acetate and lead citrate solutions were used for double staining, and the redundant solution was allowed to absorb on a clean filter paper. Finally, the microstructure of the nanohydrogel was observed through transmission electron microscopy (TEM) (JEM-1200) under the condition of 80 kV acceleration voltage.

2.10   Thermosensitive properties

The low critical solution temperature (LCST) of the PNIPAm/citral nanohydrogel was first measured visually and then verified using a differential scanning calorimeter (DSC). In the visual measurement, 10 mL of hydrogel solution was taken into a sample bottle and then placed in a constant temperature water bath at a low temperature. Each time the solution temperature was increased by 1 °C, the liquid was stabilised for

5 min, and the temperature was recorded until the solution changed from colourless and transparent to turbid. In DSC, approximately 10 mg of PNIPAm/citral nanohydrogel samples with swelling equilibrium were weighed and placed in a liquid aluminum plate, followed by DSC (AT Q2000). The resulting DSC curves were recorded to determine their LCST. The test temperature ranged from 20 °C to 50 °C, the heating rate was 5 °C min^{-1}, and deionised water was used as a reference.

2.11 *In vitro* release

Hibah *et al.*[46] studied the release of the PNIPAm/citral nanohydrogel by using dialysis bags with the corresponding adjustments. Briefly, 1 g of PNIPAm/citral nanohydrogel solution was measured in a dialysis bag and immersed in a beaker containing 100 mL of phosphate-buffered solution (0.1 mol L^{-1}, pH = 6.8). The buffer system was controlled to reach a predetermined temperature and was maintained at a constant temperature, with a stirring speed of 100 rotations per min. The release of citral was computed using the absorbance measured through UV-vis spectrophotometry after 5 mL of test buffer solution was removed within the specified time points and the same volume of fresh buffer was added (for each sampling, the absorbance was measured thrice, and the absorbance values were averaged).

2.12 PNIPAm/citral/bamboo

Firstly, the bamboo strips with a moisture content of 10% were immersed in a beaker containing PNIPAm/citral nanohydrogel and sealed in a pressurized tank. The bamboo strips were impregnated at a pressure of 0.5 MPa for 2 h. After completion, they were placed in a vacuum drying oven and dried at 30 °C until the moisture content was 10%. Finally, the bamboo strips were stored in a dryer for subsequent characterization and anti-mold treatment.

2.13 Ultraviolet-visible spectroscopy

The bamboo strips treated with PNIPAm/citral nanohydrogel were ground to obtain bamboo powder, which was dissolved in an anhydrous ethanol solution. The treated bamboo strips were scanned using a UV-1800 spectrophotometer in the wavelength range of 200–300 nm, and UV absorption spectra were obtained. The UV absorption spectra of the treated bamboo strips were compared with those of untreated bamboo strips.

2.14 X-ray diffraction

The phase composition of bamboo strips treated with the PNIPAm/citral nanohydrogel was analyzed using an X-ray powder diffractometer. The conditions for X-ray diffraction were as follows: X-ray tube, a copper target; tube voltage, 40 kV; tube current, 30 mA; scanning range of the specimen, 5–40° (2θ); and speed, 2° min^{-1}.

2.15 Anti-mold properties

The anti-mold properties of the bamboo strips uniformly treated with PNIPAm/citral nanohydrogel were tested according to the recommendations of GB/T Standard 18261.[47] The strain

suspensions of *Penicillium citrinum* (PC), *Trichoderma viride* (TV), *Aspergillus niger* (AN), and mixed molds (PC, TV, and AN mixed in a 1 : 1 : 1 ratio, abbreviated as PTA) were uniformly spread on a Petri dish containing the plate medium. Then, the dish containing the molds was cultured in an incubator at a temperature of 28 °C ± 2 °C and a relative humidity of 85% ± 5%. After the growth of the molds, a bamboo sample was placed on U-shaped glass rods in a Petri dish. The edges of the Petri dishes were sealed with a sealing film, and the dish was placed back in the incubator for 28 days for the anti-mold test. The mold infection of bamboo strips in the incubator was monitored and recorded every alternate day during the experimental period. The preventing efficiency was calculated according to the following formula (2):

$$E = \left(1 - \frac{D_1}{D_0}\right) \times 100\% \tag{2}$$

where E denotes the preventing efficiency (%); D_0 denotes the average infection levels of untreated control samples; and D_1 denotes the average infection levels of the sample treated with the agent.

3. Results and discussion

3.1 Construction of a working curve

Fig. 2(A) shows the UV-vis spectra of citral, PNIPAm, and the PNIPAm/citral nanohydrogel. As shown in the figure, the absorbance of both citral and the PNIPAm/citral nanohydrogel reached their respective peaks at 238 nm, which confirmed the presence of a characteristic UV absorption peak of citral at the selected wavelength. On the other hand, PNIPAm did not display any UV absorption, indicating that the UV spectrophotometer was suitable for the detection of citral in the PNIPAm/citral nanohydrogel. Therefore, a citral ethanol standard solution with a concentration of 2–8 μg mL^{-1} was prepared, and its absorbance was determined at 238 nm. Fig. 2(B) represents the standard curve of citral in an anhydrous ethanol solution, with the following regression equation:

$$A = 0.11353C - 0.0526 \ (R^2 = 0.99931)$$

The fitting correlation coefficient R^2 in the equation was extremely close to 1, which indicated a good linear relationship between the concentration of citral and its absorbance. Therefore, the experimental error of using this standard curve was deemed appropriate, and the content of citral could be accurately calculated.

3.2 The effect of citral concentration on EC

As depicted in Fig. 3(A), when the dosage of citral in the system was low, PNIPAm showed a minor chance of contact with citral, which is not conducive to its being embedded. With an increase in the dosage of citral, the EC gradually increased and began to decrease after reaching the maximum value because after the embedding capacity of PNIPAm was saturated, the abundance of citral was not embedded by PNIPAm and the EC was decreased. To ensure the rationality of the orthogonal
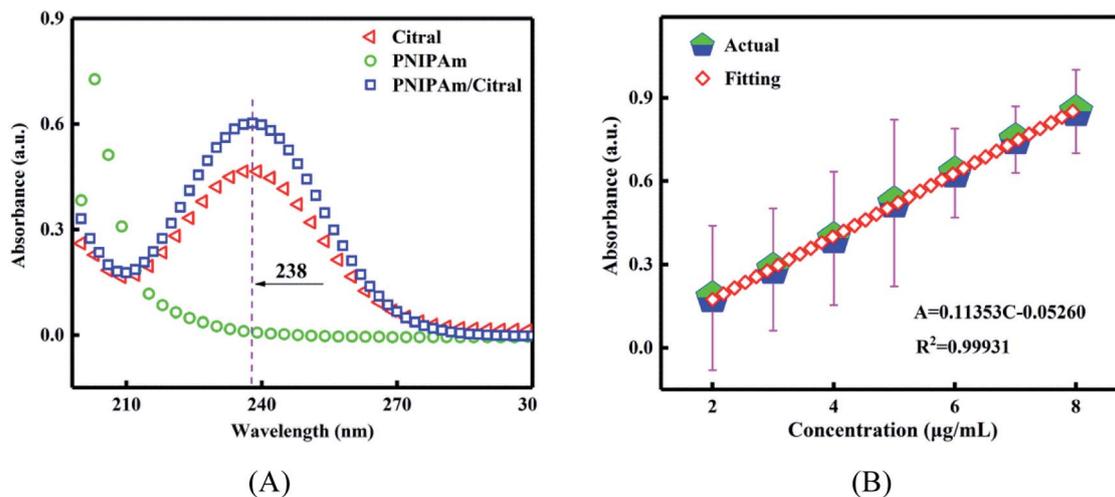
Fig. 2 (A) The UV-vis spectrogram of the PNIPAm/citral nanohydrogel. (B) The standard curve of citral in an anhydrous ethanol solution.

experimental design, we attempted to expand the numbers of horizontal intervals, and finally, 10 mg, 30 mg, and 50 mg were selected as the orthogonal experimental investigation levels.

3.3 The effect of reaction time on EC

As shown in Fig. 3(B), with an increase in the reaction time. EC first showed an increasing trend and then a decreasing trend because the encapsulation reaction system became more balanced with increasing reaction time in the beginning as more citral came in contact with and subsequently embedded in PNIPAm. However, with an increase in the reaction time, the citral not bound to PNIPAm became volatilised during the encapsulation process. On the other hand, the encapsulated citral in PNIPAm dissolved and flowed out, resulting in a decline in EC. Therefore, to obtain better EC and save the production costs, 1 h, 2 h, and 3 h were selected as the orthogonal experimental test level times.

3.4 The effects of reaction temperature on EC

As shown in Fig. 3(C), with an increase in temperature, a peak appeared in the encapsulation rate. At a temperature lower than the indoor temperature, according to the principle of Brownian motion, with an increase in temperature, the movement

frequency of citral was also increased. Consequently, the chance of contact with PNIPAm was enhanced, and finally, the EC was increased. At normal temperature, PNIPAm encapsulation of citral occurred mainly through hydrophobic interactions, and the increase in temperature made the citral molecules move intensely, thereby reducing the stability of the encapsulation complex, which was not found to be conducive to the encapsulation reaction. In addition, the excessively high temperature (beyond the LCST of PNIPAm) even led to the precipitation of PNIPAm in water. Considering that the purpose of this experiment was to obtain the solution of the PNIPAm/citral nanohydrogel, 25 °C, 30 °C, and 35 °C were selected as the orthogonal experimental investigation level temperatures.

3.5 Orthogonal experiment analysis

In line with the results of the single-factor experiments and the rational selection of the three levels for each factor, we designed the orthogonal experiment by referring to the orthogonal test table $L_9(3^4)$. Each experimental group corresponded to a citral encapsulation rate value, and the obtained orthogonal test results are shown in Table 1. k_i represents the influence of the factor i level on the EC. The higher the level of k_i, the higher is the embedding value of citral. k_{max} is the maximum of the three
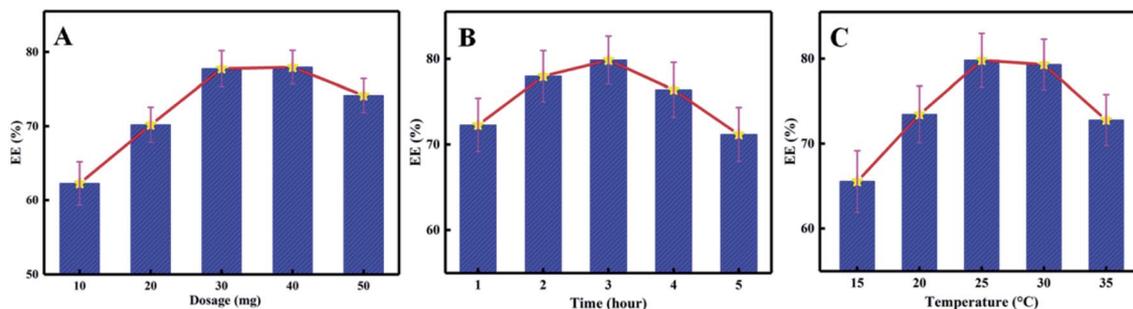

Fig. 3 The effects of dosage of citral (A), reaction time (B), and reaction temperature (C) on EC.

Table 1 Orthogonal experiment results[a]

Test no.	Factor			EC (%)
	A (mg)	B (h)	C (°C)	
1	1	1	1	62.244
2	1	2	2	65.690
3	1	3	3	60.330
4	2	1	2	79.700
5	2	2	3	80.083
6	2	3	1	82.890
7	3	1	3	63.132
8	3	2	1	74.387
9	3	3	2	64.893
k_1	62.755	68.359	73.174	
k_2	80.891	73.387	70.094	
k_3	67.471	69.371	67.848	
R	18.136	5.028	5.326	
Order	$R_A > R_C > R_B$			

[a] $R = k_{max} - k_{min}$.

k_i values of each factor, k_{min} is the minimum value, while R represents the range. The greater the value of R, the stronger is the influence on the EC.

According to the R-value in Table 1, the influences of A, B, and C on the EC were in the order: $A > C > B$. The optimal combination was $A_2B_2C_1$; thus the optimum citral dosage, reaction time, and reaction temperature were 30 mg, 2 h, and 25 °C, respectively. The verification test results indicated an average EC of 83.784%, and the error was not >0.26%. The repeatability of the experimental results was high.

The results of the variance analysis of EC are depicted in Table 2. At the 5% significance level, the effects of reaction time and reaction temperature on the EC were not found to be significant, while the dosage of citral showed a significant effect on the EC.

3.6 FT-IR analysis

As shown in the spectra of NIPAm in Fig. 4(A), the peak at 1661 cm^{-1} corresponds to the C=O stretching vibration absorption peak of the amide group, the absorption band at 1623 cm^{-1} corresponded to C=C stretching vibration of the conjugate, and the peak at 1546 cm^{-1} is the variable angle vibration caused by N–H and C–N stretching vibrations. The peak at 1462 cm^{-1} was due to –CH$_3$ unsymmetrical bending

Table 2 Variance analysis results of the EC

Source of variation	Sum of square	F value	$F_{0.05}(2, 2)$	Significance
A (mg)	531.273	60.303	19	*
B (h)	42.431	4.816	19	
C (°C)	42.886	4.868	19	
Error	8.810			
Total	625.400			

vibration, and that peak at 1170 cm^{-1} was equivalent to the contraction vibration of C–C in –CH(CH$_3$)$_2$. Finally, the peaks at 988 cm^{-1} and 910 cm^{-1}, corresponding to the hydrogen atoms on the end-enyl group swung out of the plane deformation vibration. In the spectrum of PNIPAm, the vibration peaks at 1623 cm^{-1}, 988 cm^{-1}, and 910 cm^{-1} disappeared, indicating that C=C in NIPAm was broken and that NIPAm was successfully polymerised into PNIPAm. In the spectrum of citral, the stretching vibration absorption peak of C=O in the aldehyde group was 1675 cm^{-1}. In the PNIPAm/citral chromatogram, the aldehyde group's characteristic peak disappeared, suggesting that citral was embedded in PNIPAm and that the molecular vibration was limited and hence could not show its original infrared features.[48] However, the characteristic absorption peak of the amide group at 1546 cm^{-1} was weakened, suggesting that the amide group in PNIPAm formed a hydrogen bond with the aldehyde group. The citral was firmly fixed in PNIPAm through this bond cooperation.

3.7 DLS analysis

DLS was performed to measure the hydrodynamic diameter (DH) of the PNIPAm/citral nanohydrogel prepared by the combination $A_2B_2C_1$, which displayed optimal citral encapsulation rate at room temperature. As shown in Fig. 4(B), the particle size of the PNIPAm hydrogel was within the range of 41–88 nm and that of the PNIPAm/citral hydrogel was within the range of 60–140 nm, both of which presented a normal distribution. The average particle size of the PNIPAm hydrogel was 56.1 nm, and the average particle size of the PNIPAm/citral hydrogel was 88.1 nm, which was 57.04% higher than that of the PNIPAm hydrogel. This result can mainly be attributed to the inclusion of citral nanoparticles in PNIPAm/citral nanohydrogel, which increased the volume of citral nanoparticles. Combined with our previous studies, it can be seen that the superior size of PNIPAm/citral nanohydrogel is conducive to its entry into bamboo cells to maximize its mold resistance effect.

3.8 TEM analysis

To observe the microscopic morphology of the PNIPAm/citral nanohydrogel, we characterised the prepared PNIPAm/citral nanohydrogel as having an optimal encapsulation rate of citral through TEM. As shown in Fig. 5(C), after double staining with uranyl acetate and lead citrate solution, the nanoparticles of PNIPAm/citral hydrogel were visible with a relatively uniform dispersion, and the visual average particle size was consistent with that observed in DLS, which confirmed the reliability of the experimental results. As depicted clearly in Fig. 5(D), the shape of the PNIPAm/citral nanohydrogel observed under TEM was spherical, and citral was completely encapsulated in the PNIPAm hydrogel, which formed a core–shell structure, with citral as the 'core' and PNIPAm as the 'shell'. PNIPAM as the 'shell' could protect citral and eliminate the drawbacks of citral itself to a certain extent. In addition, a small amount of citral could be encapsulated by the PNIPAm hydrogel and remain free in the entire hydrogel system.
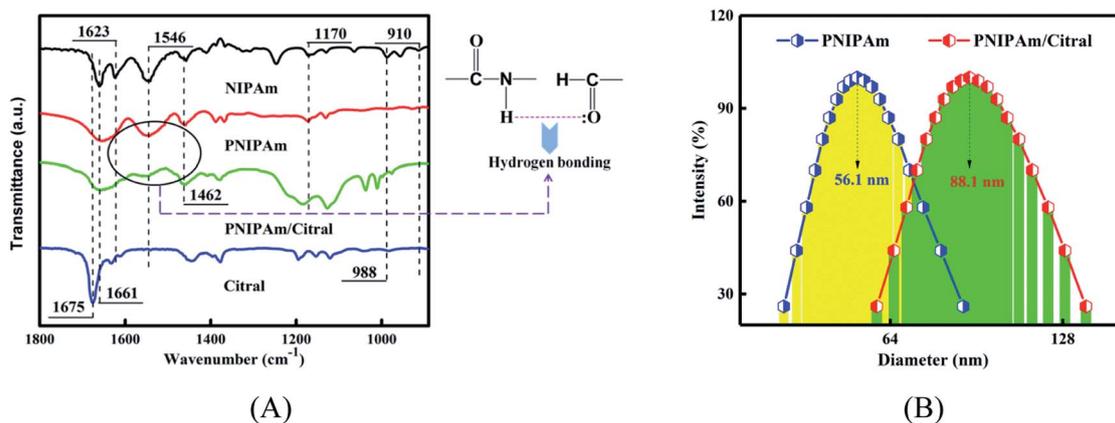
(A)   (B)

Fig. 4   The FT-IR (A) and DH distribution (B) of the PNIPAm/citral nanohydrogel.
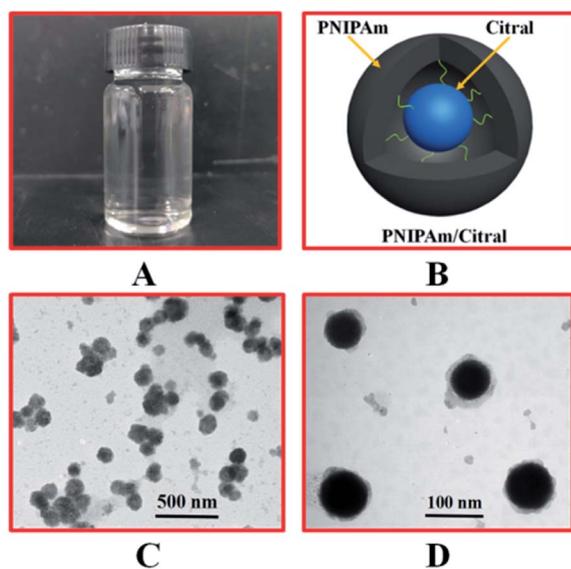

Fig. 5   (A) The sample of PNIPAm/citral nanohydrogel. (B) A schematic diagram of the core–shell structure of the PNIPAm/citral nanohydrogel. (C) and (D) TEM images of the PNIPAm/citral nanohydrogel with 500 nm and 100 nm scales.

3.9   Thermosensitive properties

From the perspective of when the temperature of the PNIPAm hydrogel solution increased to LCST, the hydration of the hydrogel molecular chain was weakened and micelles were formed by contraction, such that the appearance of the hydrogel solution changed from colourless and transparent to turbid. Therefore, the LCST of the PNIPAm/citral nanohydrogel with the best citral encapsulation rate determined using the visual method was 36 °C. To determine the repeatability of the phase transition of the PNIPAm/citral nanohydrogel, the 'Heat–Cool–Heat' cycle was conducted on the sample solution and the turbidity of the solution was recorded. Although the visual method is simple and effective and allows the direct observation of the phase-transition phenomenon of hydrogels, some errors were noted in the observation process and the measurement

results were not sufficiently accurate. Since the volumetric phase transition of PNIPAm is a phase-separation process that must be accompanied by specific phase-transition heat,[49] we verified the visually obtained results by using DSC; the results are depicted in Fig. 6(A).

As depicted in Fig. 6(A), the LCST of both PNIPAm and the PNIPAm/citral nanohydrogel was 35.4 °C, which revealed a clear and transparent appearance at a temperature lower than the LCST because PNIPAm formed hydrogen bonds with water and dissolved in water. When the temperature increased to 35.4 °C, the appearance changed to white and turbid, which was reversible, because the hydrogen bonds were destroyed by the heat energy and the nanohydrogel precipitated from water under the action of hydrophobic groups. However, when compared with the DSC curve of PNIPAm, the LCST range of PNIPAm/citral nanohydrogel was wider and the peak shape was flatter, due to the addition of hydrophilic PEGMS that plays a role in solubilising PNIPAm and in turn makes the LCST range of the PNIPAm/citral nanohydrogel wider.[50] In general, the results obtained through the DSC and visual method indicated that the PNIPAm/citral nanohydrogel possesses excellent hydrophilicity and thermosensitive properties, which lay a solid research foundation for the sustained release of citral.

3.10   Release characteristics

To investigate the kinetics of release for the PNIPAm/citral nanohydrogel at different temperatures, we prepared the PNIPAm/citral nanohydrogel with the best citral encapsulation rate and conducted release experiments at different temperatures. As shown in Fig. 6(B), the release rate of the PNIPAm/citral nanohydrogel was significantly affected by temperature. For instance, at 25 °C, the release rate of PNIPAm/citral nanohydrogel was slow and could reach only 13.67% at 48 h, whereas when the temperature was increased to 36 °C, the citral was completely released after 48 h. From the PNIPAm/citral release curve fitting, we concluded that its release mechanism parameters were 0.97587 and 0.99232 (*i.e.*, close to 1) at 25 °C and 36 °C, respectively. Thus, the PNIPAm/citral nanohydrogel's release of citral at 25 °C was in line with the zero-order release
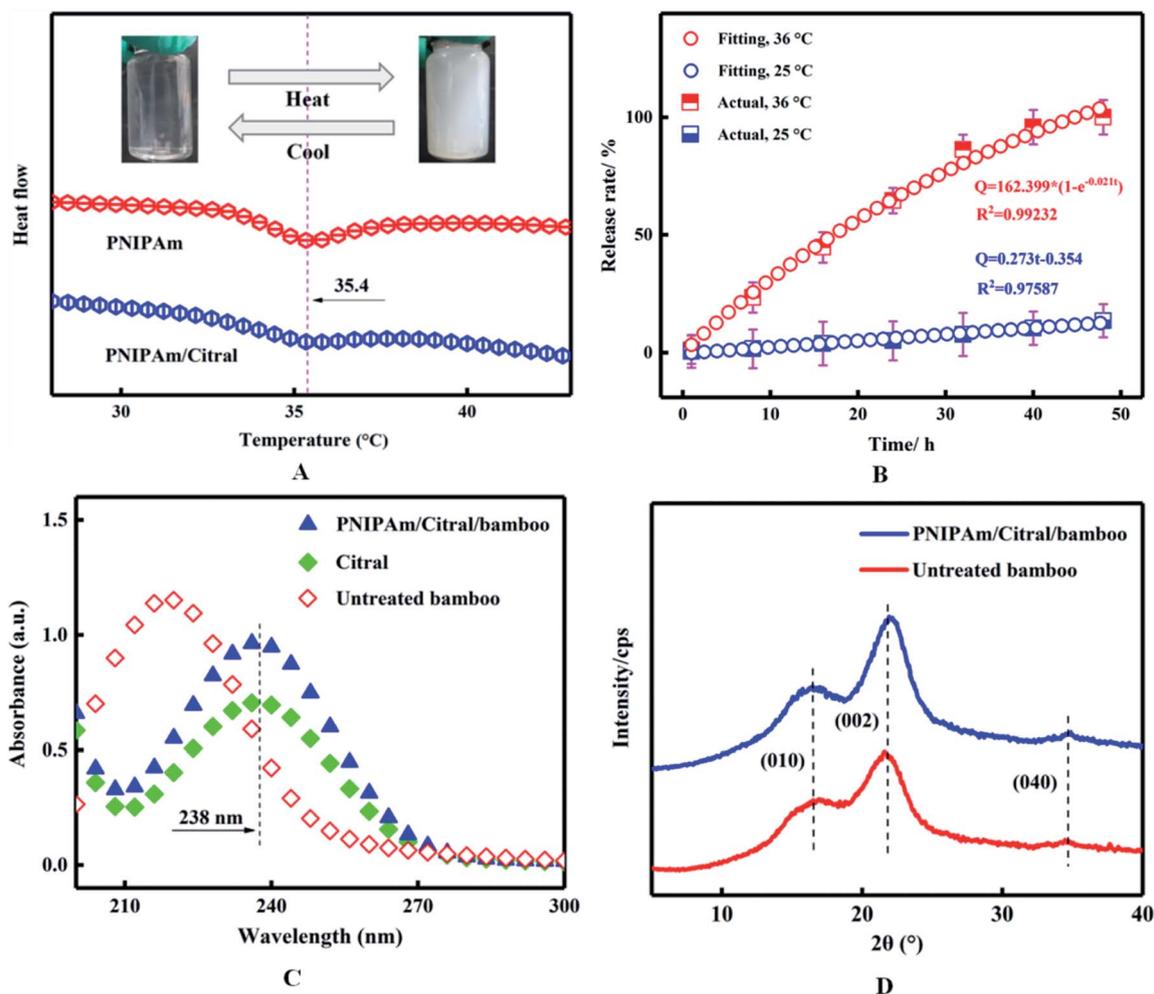
Fig. 6 The thermosensitive properties (A) and release properties (B) of PNIPAm/citral nanohydrogel. UV–vis spectra (C) and XRD patterns (D) of PNIPAm/citral/bamboo.

kinetics equation, thereby conforming to the first-order kinetics equation at 36 °C (ref. 51) and further proving its perfect release properties.

Cumulatively, our study proposes a method for the preparation of PNIPAm/citral hydrogel nanoparticles, with effective embedding of citral in the PNIPAm polymer layer, while avoiding the oxidation and volatilisation of the final product as well as significantly improving the hydrophilicity and stability of citral. The reuse of PNIPAm thermosensitive properties to realise the control of citral release can thus meet the requirements of different industries.

3.11 UV-vis analysis

The ultraviolet absorption spectra of PNIPAm/citral/bamboo were obtained through UV-vis scanning and compared with the spectra of untreated bamboo strips and citral. In previous characterisation, we confirmed that citral was encapsulated by PNIPAm to form PNIPAm/citral nanohydrogel. As shown in Fig. 6(C), the characteristic absorption peak of citral did not appear at 238 nm, which indicated the absence of

PNIPAm/citral nanohydrogel in the untreated bamboo strips. Conversely, the characteristic absorption peak of the PNIPAm/citral/bamboo appeared at 238 nm, which indicated that the PNIPAm/citral nanohydrogel was successfully bound to bamboo after the pressure impregnation treatment. Notably, the characteristic absorption peak of citral in PNIPAm/citral nanohydrogel appeared in the ultraviolet spectrum, which was due to the good solubility of citral and PNIPAm in anhydrous ethanol, and PNIPAm did not interfere with the UV absorption of citral.

3.12 XRD analysis

The XRD patterns of PNIPAm/citral/bamboo are shown in Fig. 6(D). As seen from the figure, the positions of the diffraction peaks, (010), (002), and (040), of the PNIPAm/citral/bamboo and the untreated bamboo strips were roughly similar to those of the cellulose I crystal, which indicated that the original crystalline structure of the bamboo strips was not damaged after the impregnation with PNIPAm/citral nanohydrogel. Moreover, because of the presence of a physical bond between the inclusion compound and bamboo, the impregnation of

PNIPAm/citral nanohydrogel did not change the dimensional stability of bamboo strips.

3.13 Anti-mold properties

Fig. 7(C) shows that the bamboo strips in the control group (untreated) were infected with *P. oryzae* (PC), TV, AN, and a mix of the three fungi (PTA); their surfaces were mostly covered with a fungus and their colour changed, therefore, the untreated bamboo had no antifungal properties. In contrast, as depicted in Fig. 7(D), the surface of the bamboo strips treated with the PNIPAm/citral nanohydrogel was hardly infected by PC, TV, AN, or PTA, and they mostly retained the original colour. The infection level of the four fungi to the control group bamboo strips was as high as 4, as shown in Fig. 7(A); on the other hand, after treatment with PNIPAm/citral nanohydrogel, the infection level of the treated bamboo strips by all fungi was below 1 after 28 days, as shown in Fig. 7(B). This outcome can be explained mainly from the following two perspectives: first, citral can change the shape of its mycelium and destroy the integrity of the mycelium structure, cell wall, and cell membrane structure, thereby causing leakage of nucleic acids, proteins, and other substances in the cell as well as destroying the pH balance inside and outside of the cell to inhibit or kill mold.[42] Second, owing to the release characteristics of PNIPAm/citral nanohydrogel, which enable the continuous release of citral on the NIPAm polymer carrier, it maintained a constant citral concentration in the system to ensure a long-term antibacterial effect.

4. Conclusion

In this study, the core–shell type PNIPAm/citral nanohydrogel was prepared using a simple strategy of SFEP and under warm reaction conditions, which resulted in an encapsulation efficiency of 83.784% after optimisation. The nanohydrogel displayed superior hydrophilic and thermal responsiveness and release characteristics. After the high-pressure impregnation of bamboo strips with the nanohydrogel, the infection levels of the bamboo strips by common molds, all below 1, and the dosage of citral were greatly reduced. The presented approach is extremely beneficial in terms of the improved effectiveness of bamboo
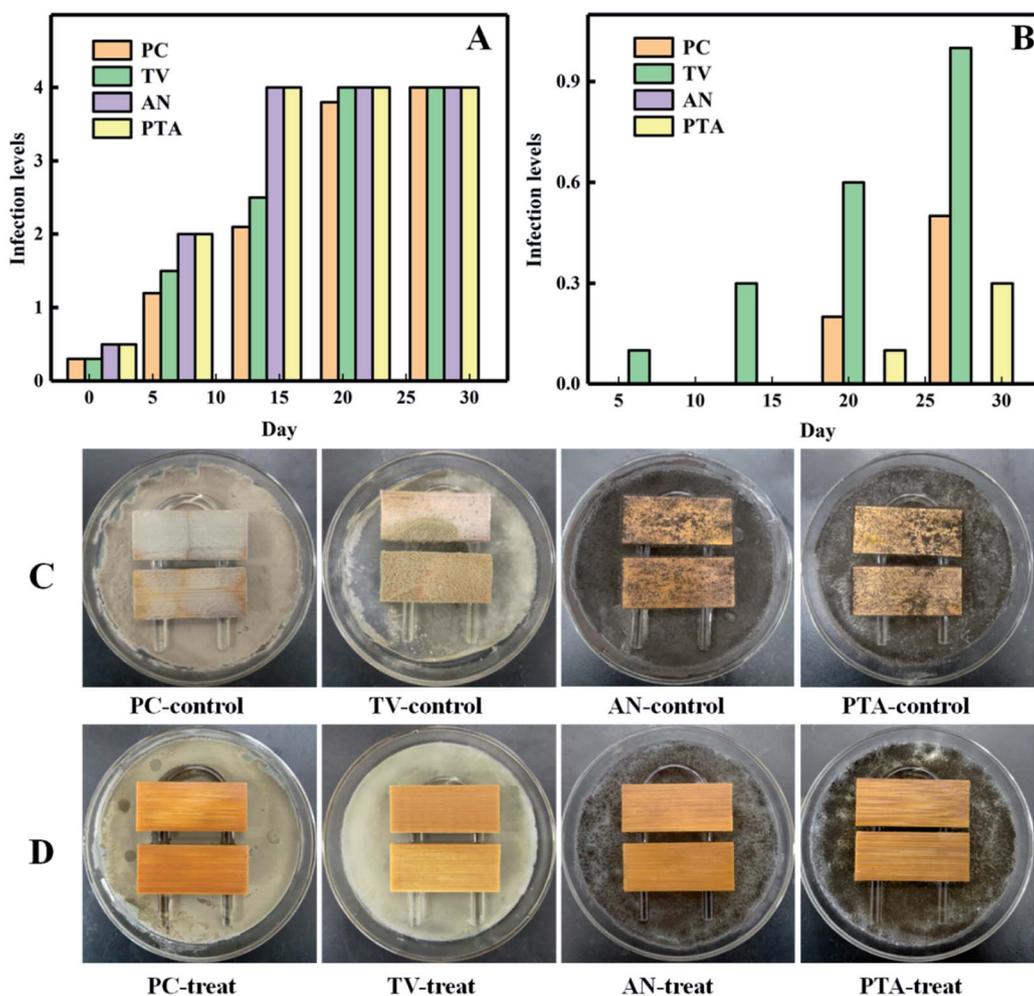

Fig. 7 The infection levels of the control group (A) and treatment group (B). The anti-mold results of the control group (C) and treated group (D) on the 28th day.

against mold, and the cost is reduced for their industrial application. Our results suggest that this eco-friendly, safe, and highly efficient thermal-sensitive nanohydrogel can be used as a mold coating for bamboo, and even applied to other biomass materials in addition to bamboo.

Author contributions

Rui Peng and Chungui Du are co-first authors of the article. Or Rui Peng and Chungui Du contribute equally to the article.

Conflicts of interest

The authors declare no competing financial interest.

Acknowledgements

References

1 U. G. K. Wegst and M. F. Ashby, *Philos. Mag.*, 2004, **84**, 2167–2186.

2 S. Amini and A. Miserez, *Acta Biomater.*, 2013, **9**, 7895–7907.

3 Z. Liu, Z. Zhang and R. O. Ritchie, *Adv. Funct. Mater.*, 2020, **30**, 1908121.

4 Z. Li, C. Chen, R. Mi, W. Gan and L. Hu, *Adv. Mater.*, 2020, **32**, 1906308.

5 C. Chaoji, Z. Li, R. Mi, J. Dai, H. Xie, Y. Pei, J. Li, H. Qiao, H. Tang, B. Yang and L. Hu, *ACS Nano*, 2020, **14**, 1–29.

6 S. A. Kelchner, *Mol. Phylogenet. Evol.*, 2013, **67**, 404–413.

7 J. Li, Z. Wu, Y. Bao, Y. Chen, C. Huang, N. Li, S. He and Z. Chen, *J. Saudi Chem. Soc.*, 2017, **21**, 920–928.

8 J. Chen, Y. Ma, H. Lin, Q. Zheng, X. Zhang, W. Yang and R. Li, *Coatings*, 2018, **9**, 15.

9 W. Li, L. Chen, Y. Li and X. Li, *J. Wood Chem. Technol.*, 2020, **40**, 126–135.

10 D. Ren, J. Li, Y. Bao, Z. Wu, S. He, A. Wang, F. Guo and Y. Chen, *Colloids Surf., A*, 2018, **555**, 381–388.

11 R. Muthusamy, K. Yrjälä, K. Vinod, A. Sharma, J. Cho, V. Satheesh and Z. Mingbing, *Food and Energy Security*, 2020, **9**, 1–36.

12 J. Li, H. Yu, Z. Wu, J. Wang, S. He, J. Ji, N. Li, Y. Bao, C. Huang, Z. Chen, Y. Chen and C. Jin, *Colloids Surf., A*, 2016, **508**, 117–123.

13 M. Liu, W. Li, F. Guo, H. Wang, X. Zhang and Y. Yu, *Constr. Build. Mater.*, 2021, **276**, 122156.

14 J. Zhang, Q. Huang, C. Du, R. Peng, Y. Hua, Q. Li, A. Hu and J. Zhou, *Molecules*, 2020, **25**, 4135.

15 Y. Wang, X. Sun, Y. Ding, Z. Fei, C. Jiao, M. Fan, B. Yao, P. Xin, J. Chu and Q. Wei, *J. Exp. Bot.*, 2019, **70**, 3911–3926.

16 H. Zhao, S. Zhao, B. Fei, H. Liu, H. Yang, H. Dai, D. Wang, W. Jin, F. Tang, Q. Gao, H. Xun, Y. Wang, L. Qi, X. Yue, S. Lin, L. Gu, L. Li, T. Zhu, Q. Wei, Z. Su, T. Wan, D. A. Ofori, G. M. Muthike, Y. M. Mengesha, E. S. R. M. de Castro, A. L. Beraldo, Z. Gao, X. Liu and Z. Jiang, *GigaScience*, 2017, **6**, 1–7.

17 Z. Wu, D. Huang, W. Wei, W. Wang, X. Wang, Q. Wei, M. Niu, M. Lin, J. Rao and Y. Xie, *J. Cleaner Prod.*, 2019, **209**, 273–282.

18 J.-K. Liu, R. Phookamsak, E. B. G. Jones, Y. Zhang, T. W. Ko-Ko, H.-L. Hu, S. Boonmee, M. Doilom, E. Chukeatirote, A. H. Bahkali, Y. Wang and K. D. Hyde, *Fungal Divers.*, 2011, **51**, 135–154.

19 D. Q. Dai, R. Phookamsak, N. N. Wijayawardene, W. J. Li, D. J. Bhat, J. C. Xu, J. E. Taylor, K. D. Hyde and E. Chukeatirote, *Fungal Divers.*, 2017, **82**, 1–105.

20 D. Cheng, S. Jiang and Q. Zhang, *Eur. J. Wood Wood Prod.*, 2013, **71**, 143–145.

21 L. Yang, Z. Lou, X. Han, J. Liu, Z. Wang, Y. Zhang, X. Wu, C. Yuan and Y. Li, *Mater. Today Commun.*, 2020, **23**, 101086.

22 Z. Aytac, A. Celebioglu, Z. I. Yildiz and T. Uyar, *Nanomaterials*, 2018, **8**, 793.

23 M. Ferrario, D. Fenoglio, A. Chantada and S. Guerrero, *Int. J. Food Microbiol.*, 2020, **332**, 108811.

24 P. A. Bhat, N. Nazir, O. A. Chat and A. A. Dar, *Food Chem.*, 2021, **340**, 128168.

25 J. Cao, H. Liu, Y. Wang, X. He, H. Jiang, J. Yao, F. Xia, Y. Zhao and X. Chen, *Food Control*, 2021, **120**, 107507.

26 D. Ailincai, L. Tartau Mititelu and L. Marin, *Drug Delivery*, 2018, **25**, 1080–1090.

27 Y. Zhang, J. Wei, H. Chen, Z. Song, H. Guo, Y. Yuan and T. Yue, *LWT*, 2020, **117**, 108667.

28 V. Weisheimer, D. Miron, C. B. Silva, S. S. Guterres and E. E. Schapoval, *Pharmazie*, 2010, **65**, 885–890.

29 D. Natrajan, S. Srinivasan, K. Sundar and A. Ravindran, *J. Food Drug Anal.*, 2015, **23**, 560–568.

30 J. Wang, S. Oussama Khelissa, N.-E. Chihib, E. Dumas and A. Gharsallaoui, *Food Chem.*, 2019, **298**, 125079.

31 H. Tian, Z. Lu, D. Li and J. Hu, *Food Chem.*, 2018, **248**, 78–85.

32 J. Lee, K. H. Ku, M. Kim, J. M. Shin, J. Han, C. H. Park, G.-R. Yi, S. G. Jang and B. J. Kim, *Adv. Mater.*, 2017, **29**, 1700608.

33 L. Tang, L. Wang, X. Yang, Y. Feng, Y. Li and W. Feng, *Prog. Mater. Sci.*, 2021, **115**, 100702.

34 H. Kim, S.-M. Jo, F. Meng, Y. Guo, H. Thérien-Aubin, R. Golestanian, K. Landfester and E. Bodenschatz, *Adv. Funct. Mater.*, 2020, **30**, 2006019.

35 L. G. S. Garcia, M. G. da Rocha, L. R. Lima, A. P. Cunha, J. S. de Oliveira, A. R. C. de Andrade, N. M. P. S. Ricardo, W. A. Pereira-Neto, J. J. C. Sidrim, M. F. G. Rocha, R. S. Vieira and R. S. N. Brilhante, *Int. J. Biol. Macromol.*, 2021, **166**, 621–632.

36 S. J. Choi, E. A. Decker, L. Henson, L. M. Popplewell and D. J. McClements, *J. Agric. Food Chem.*, 2009, **57**, 11349–11353.

37 S. J. Choi, E. A. Decker, L. Henson, L. M. Popplewell and D. J. McClements, *J. Food Sci.*, 2010, **75**, C536–C540.

38 X. Yang, H. Tian, C.-T. Ho and Q. Huang, *J. Agric. Food Chem.*, 2012, **60**, 402–409.

39 W. Jinguang, Y. Huilong, L. Hongzhi, D. Chungui, Z. Zhongxi, H. Qiuli and Y. Xiaoling, *J. Mater. Sci.*, 2018, **53**, 12056–12064.

40 J. Gao and B. J. Frisken, *Langmuir*, 2003, **19**, 5212–5216.

41 J. Gao and B. J. Frisken, *Langmuir*, 2005, **21**, 545–551.

42 J. Zhang, C. Du, Q. Li, A. Hu, R. Peng, F. Sun and W. Zhang, *R. Soc. Open Sci.*, 2021, **8**, 202244.

43 X. Hu, B. Wei, H. Li, C. Wu, Y. Bai, X. Xu, Z. Jin and Y. Tian, *Carbohydr. Polym.*, 2012, **90**, 1193–1196.

44 X. Liu, M. Chen and B. Xie, *Jiangxi Chemical Industry*, 2001, 17–20.

45 K. B. Almeida, J. L. Araujo, J. F. Cavalcanti, M. T. V. Romanos, S. C. Mourão, A. C. F. Amaral and D. Q. Falcão, *Rev. Bras. Farmacogn.*, 2018, **28**, 495–502.

46 H. M. Aldawsari, S. M. Badr-Eldin, G. S. Labib and A. H. El-Kamel, *Int. J. Nanomed.*, 2015, **10**, 893–902.

47 *Test method for anti-mildew agents in controlling wood mould and stain fungi, GB/T 18261-2013*, 2013.

48 Z. A. Haiyee, N. Saim, M. Said, R. M. Illias, W. A. W. Mustapha and O. Hassan, *Food Chem.*, 2009, **114**, 459–465.

49 A. Qin, M. Lv, Q. Liu and P. Zhang, *Appl. Chem.*, 2006, **23**, 581–585.

50 C. K. Nisha, D. Dhara and P. R. Chatterji, *J. Macromol. Sci., Part A: Pure Appl.Chem.*, 2000, **37**, 1447–1460.

51 H. Wu, H. Liang, Q. Yuan, T. Wang and X. Yan, *Carbohydr. Polym.*, 2010, **82**, 613–617.